Relativistic suppression of Auger recombination in Weyl semimetals

A. N. Afanasiev,[1,2,*] A. A. Greshnov,[1,2] and D. Svintsov[2]
[1]*Ioffe Institute, St. Petersburg 194021, Russia*
[2]*Moscow Institute of Physics and Technology, Dolgoprudny 141700, Russia*

(Received 13 November 2018; published 4 March 2019)

Auger recombination (AR) being electron-hole annihilation with energy-momentum transfer to another carrier is believed to speed up in materials with small band gap. We theoretically show that this rule is violated in gapless three-dimensional materials with ultrarelativistic electron-hole dispersion, Weyl semimetals (WSMs). Namely, AR is prohibited by energy-momentum conservation laws in *prototypical* WSM with a single Weyl node, even in the presence of anisotropy and tilt. In *real* multinode WSMs, the geometric dissimilarity of nodal dispersions enables weak *internode* AR, which is further suppressed by strong screening due to large number of nodes. While partial AR rates between the nodes of the same node group are mutually equal, the intergroup processes are nonreciprocal, so that one of the groups is *geometrically protected* from AR. This geometrical protection prolongs AR lifetime up to two orders of magnitude, to the level of nanoseconds.

DOI: 10.1103/PhysRevB.99.115202

I. INTRODUCTION

The latest years of condensed-matter physics are marked by an intense search for solid-state realizations of exotic fundamental particles [1–3]. The unique electronic properties of graphene [4], Weyl [5–8], and Dirac [9,10] semimetals enabled the tabletop observation of Klein tunneling [11], supercritical atomic collapse [12], axial [13], and axial-gravitational [14] anomalies. In this strive for high-energy physics *enabled* by electronic properties of novel materials, less attention is paid to the effects *prohibited* by these properties. Such negatory search still can be fruitful. In particular, suppression of electron scattering, relaxation, and recombination in solids [15–17] would enable the observation of new phases of ultraclean matter, needless to say ultrafast electronic and photonic devices.

In this paper, we show that quasirelativistic dispersion of fermions in recently discovered Weyl semimetals (WSMs) strongly suppresses the electron-hole recombination with energy-momentum transfer to another carrier, known as Auger recombination (AR). The AR is among the key obstacles toward the realization of nonequilibrium phases of electron-hole liquid [18], excitonic [19], and Floquet topological insulators [20]. In addition, AR is the primary "killer" of population inversion and optical gain in narrow-gap semiconductor lasers [21,22] hindering their promotion into terahertz range. Numerous attempts to suppress AR invoked strain engineering [23], modification of wave-function profiles [24], and exchange effects upon scattering [25]. However, there has been no materials with "natural" AR suppression as it occurs in WSM.

We further elaborate the incompleteness of analogy between relativistic electrons and Weyl fermions, and reveal its consequences for AR. In real WSMs, there exist multiple Weyl nodes located at *low-symmetry* points of the Brillouin zone (Fig. 1), which can be attributed to one or several node groups (W_1 and W_2 in the TaAs family). As a result, the carrier energy spectrum acquires anisotropy [26–28] and tilt. We show that it is the dissimilarity of energy spectra at different nodes that enables weak *internode* recombination, while the *intranode* AR remains prohibited. Similar intervalley AR was noted for lead salts [29]; however, strong suppression of intravalley process was not realized. Adopting the relation between the recombination and dissipative parts of polarizability [30], we derive an illustrative geometric construction for evaluation of AR. We use it to reveal the key features of interband population inversion dynamics. The most intriguing one is nonreciprocity of AR between various node groups, and suppression of AR at nodes with fast carrier velocity, which we call *geometrically protected population inversion*. This protection, along with strong screening due to large number of nodes, prolongs the nonradiative lifetimes up to the level of several nanoseconds.

II. AUGER RECOMBINATION IN PROTOTYPICAL WEYL SEMIMETAL

The suppression of AR in WSMs is tightly linked to the impossibility of impact ionization of Dirac vacuum by high-energy electrons [31]. Indeed, an electron with energy-momentum relation $E^2 = (mv_0^2)^2 + (kv_0)^2$ cannot emit electron-positron pairs due to nonequal energies of initial (mv_0^2) and final states ($\geqslant 3mv_0^2$) in the center-of-mass system.

As the mass gap tends to zero and dispersion becomes *ultrarelativistic*, $E(\mathbf{k}) = kv_0$, the situation becomes pathological. Momentum conservation for the Auger process reads $\mathbf{k}_{e1} + \mathbf{k}_{h1} + \mathbf{k}_{e2} = \mathbf{k}'_{e2}$, where $\mathbf{k}_{e1}$ and $\mathbf{k}_{h1}$ are the momenta of recombining electron and hole (counterpart of positron in solids), and $\mathbf{k}_{e2}$ and $\mathbf{k}'_{e2}$ are the initial and final momenta of the "hot" electron. The energy conservation implies

*afanasiev.an@mail.ru

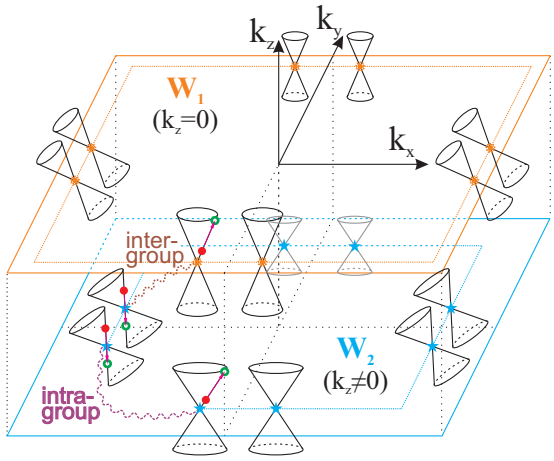

FIG. 1. Schematic structure of the Weyl nodes and internode AR in the TaAs family of WSMs having C_{4v} point symmetry with two groups of the nodes, known as W_1 and W_2. Wavy lines show the two types of Auger processes involving two nodes of the same group or the nodes of different groups. In the latter case, the interband transition occurs in W_1 and the intraband one in W_2 (or vice versa).

$k_{e1} + k_{h1} + k_{e2} = k'_{e2}$, and renders all four momenta collinear. The phase space for collinear collisions vanishes. However, the interaction strength between collinear carriers diverges as their unidirectional motion with equal velocities implies infinite interaction time. This fact is known as collinear scattering anomaly [32], and the resulting AR probability of the form $0 \times \infty$ was shown to be finite in two dimensions [33–36].

To put the solution of the AR problem in three dimensions on solid ground, we use a transparent yet not widely adopted relation [30] between the recombination and imaginary parts of inter- and intraband polarizations, $\mathrm{Im}\Pi_{-+}$ and $\mathrm{Im}\Pi_{ss}$ (here $s = \pm 1$ is the index of conduction and valence bands). The AR rate in this formalism involves the product of electron-hole annihilation probability characterized by $\mathrm{Im}\Pi_{-+}$, the squared amplitude of virtual photon propagation, and the probability of interband photon absorption $\mathrm{Im}\Pi_{ss}$. The formal expression for the rate of AR with energy transferred to the sth band, $\mathcal{R}^{(s)}$, reads

$$\mathcal{R}^{(s)} = 4\sum_{\mathbf{q}\omega} \mathrm{Im}\Pi_{-+}(\omega,\mathbf{q})\frac{|V_0(q)|^2}{|\epsilon(\omega,\mathbf{q})|^2}\mathrm{Im}\Pi_{ss}(\omega,\mathbf{q}) \times [n_B(\omega - \Delta\mu_{eh}) - n_B(\omega)], \quad (1)$$

where $V_0(\mathbf{q}) = 4\pi e^2/q^2$ is the Fourier transform of Coulomb interaction, $\epsilon(\omega,\mathbf{q})$ is the dielectric function of WSMs, $n_B(\omega) = [e^{\omega/T} - 1]^{-1}$ is the Bose distribution, and $\Delta\mu_{eh} = \mu_e - \mu_h$ is the difference of electron and hole quasi-Fermi levels [37]. Summation in (1) is performed over all possible frequencies ω and wave vectors $\mathbf{q}$ of virtual photons, $\sum_{\mathbf{q}\omega} \equiv (2\pi)^{-4}\int d^3\mathbf{q}\, d\omega$.

Since AR involves both inter- and intraband electron transitions, the domains of nonzero $\mathrm{Im}\Pi_{-+}$ and $\mathrm{Im}\Pi_{ss}$ should intersect in $(\omega,\mathbf{q})$ 4-space. However, the interband emission is bound inside the "excitation cone," $\omega \geqslant v_0 q$, while intraband absorption is possible only outside of it, $\omega \leqslant v_0 q$, as

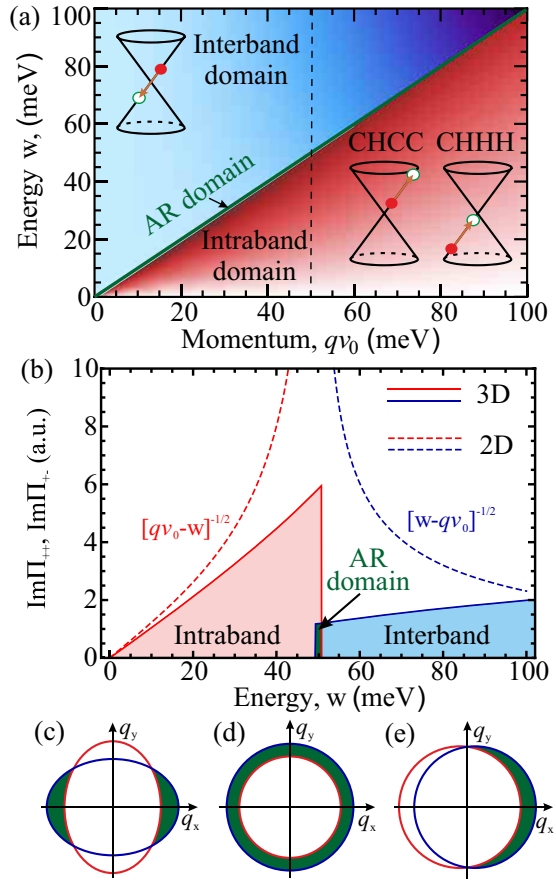

FIG. 2. Strong suppression of AR in WSMs explained in terms of overlap between intra- and interband excitations. (a) Color maps of inter- ($\mathrm{Im}\Pi_{-+}$) and intraband ($\mathrm{Im}\Pi_{ss}$) polarizabilities that are nonzero on different sides of the $\omega = v_0 q$ line in prototypical WSMs. (b) Frequency dependence of polarizations at $qv_0 = 50$ meV. Dashed lines show the respective polarizations for 2D graphene. (c)–(e) Overlap of the interband and intraband domains of different nodes in WSMs in the $\mathbf{q}$ space at fixed frequency ω (q_z is omitted for simplicity) in the cases of anisotropy (c), velocity difference (d), and tilt (e).

follows from conservation laws for single-particle processes [Fig. 2(a)]. In a formal language:

$$\mathrm{Im}\Pi^{(0)}_{-+} = F_{-+}(\omega, q)\theta(\omega - v_0 q), \quad (2)$$

$$\mathrm{Im}\Pi^{(0)}_{ss} = F_{ss}(\omega, q)\theta(v_0 q - |\omega|), \quad (3)$$

where $\theta(x)$ is the unit step function and $F_{ss'}(\omega, q)$ are smooth [38]. Integration of smooth functions in (1) over the region of zero measure results in zero value of $\mathcal{R}^{(s)}$ [see Fig. 2(b)]. It contrast to the two-dimensional case [upper curves in Fig. 2(b)] where $F_{ss'}(\omega, q)$ possess square-root singularities at $\omega = v_0 q$, which resulted in finite AR rate [33,35]. One may speculate that the fraction of collinear carriers among all electrons and holes is considerably greater in two dimensions (2D) than in three dimensions.

The above arguments concerning AR suppression apply to any three-dimensional materials with linear gapless energy-momentum relation. These could be both topological Weyl

and Dirac semimetals, as well as materials with accidental band degeneracy [39]. In Dirac semimetals Na_3Bi [9] and Cd_3As_2 [10], there exist two mirror-symmetric Dirac cones on the k_z axis of the Brillouin zone, and the AR channel opens up only due to deviations from linear dispersion or carrier-carrier scattering [36]. In WSMs, there exist multiple anisotropic Weyl nodes at low-symmetry points of the Brillouin zone. Below we shall prove that an AR channel opens up in multinode WSMs even within the linear band approximation.

III. AUGER RECOMBINATION IN REAL WEYL SEMIMETAL

To study AR in materials with general anisotropic Weyl velocity tensor $\hat{v}_n$ and tilt velocity $\mathbf{u}_n$ (which are specific to the Weyl node group, W_n), we introduce the Hamiltonian

$$H_n(\mathbf{k}) = \mathbf{w}_n(\mathbf{k})\boldsymbol{\sigma} + w_n^{(t)}(\mathbf{k})\sigma_0, \tag{4}$$

where $\mathbf{w}_n(\mathbf{k}) = \hat{v}_n\mathbf{k}$ and $w_n^{(t)}(\mathbf{k}) = \mathbf{u}_n\mathbf{k}$. Its eigenvalues are

$$E_{n,s}(\mathbf{k}) = s|\mathbf{w}_n(\mathbf{k})| + w_n^{(t)}(\mathbf{k}). \tag{5}$$

Explicit forms of dispersion in the nodes of the group are given by $E_{n,s}^{(i)}(\mathbf{k}) = E_{n,s}(g_n^{(i)}\mathbf{k})$, where $g_n^{(i)}$ represent operations of the point group connecting the nodes (C_{4v} for the TaAs family; Fig. 1).

Linearity of Hamiltonian (4) in momentum operators allows one to relate the polarization of the anisotropic tilted ith node $\Pi_{ss'}^{(i)}$ and the polarization of the prototypical isotropic WSM $\Pi_{ss'}^{(0)}$, via a linear coordinate transform

$$\Pi_{ss'}^{(i)}(\omega, \mathbf{q}) = \Pi_{ss'}^{(0)}\big(\omega - \mathbf{u}_n g_n^{(i)}\mathbf{q}, v_n^{-1}\hat{v}_n g_n^{(i)}\mathbf{q}\big), \tag{6}$$

where $v_n = |\det \hat{v}_n|^{1/3}$ is the average Weyl velocity. This transform implies that anisotropy and tilt of dispersion translates in the respective deformation of the excitation cone. As a result, the inter- and intraband excitations within the same node still do not overlap in the presence of tilt and anisotropy, and intranode AR remains forbidden.

At the same time, deformation of the Weyl cones opens up the internode recombination channel. Geometrically, the overlap between inter- and intraband excitations in different nodes can be produced both by different orientation of velocity tensors, tilt, and different absolute values of Weyl velocity (in multigroup WSMs). These possibilities are illustrated in Figs. 2(c)–2(e). As long as the difference in dispersion of the nodes is small, the *partial* AR rate involving the nodes i and j, $R_{ij}^{(s)}$, can be factorized into the *geometric* and *statistical* parts [38],

$$R_{ij}^{(s)} = \mathcal{G}_{ij}^{(s)}\mathcal{S}_{ij}^{(s)}. \tag{7}$$

The dimensionless geometric factor $\mathcal{G}$ originates from integration of the Coulomb amplitude $V_0(\mathbf{q})$ over the allowed wave vectors [shaded areas in Figs. 2(c)–2(e)]. Mathematically, it is given by an integral over the solid angle of a unit vector $\mathbf{e_q}$,

$$\mathcal{G}_{ij}^{(s)} = \int_{\Delta(\mathbf{e_q})>0} \frac{\Delta(\mathbf{e_q})d\mathbf{e_q}}{\left|v_n\left[g_n^{(i)}\right]^{-1}\hat{v}_n^{-1}\mathbf{e_q}\right|^4}, \tag{8}$$

$$\Delta(\mathbf{e_q}) = \left|\hat{v}_{n'}g_{ij}\hat{v}_n^{-1}\mathbf{e_q}\right| - 1 - (\mathbf{u}_n - \mathbf{u}_{n'}g_{ij})\hat{v}_n^{-1}\mathbf{e_q}, \tag{9}$$

where $g_{ij} = g_{n'}^{(j)}[g_n^{(i)}]^{-1}$, and the nodes i, j are assumed to belong to the groups $W_{n,n'}$, respectively.

Once a small difference in node dispersions is carried to $\mathcal{G}$, the statistical factor $\mathcal{S}$ is expressed via the polarization of the prototypical WSM,

$$\mathcal{S}_{ij}^{(s)} = \int \frac{\omega_\mathbf{q} d^3\mathbf{q}}{16\pi^5}|\tilde{V}(q)|^2 F_{-+}^{(i)}(\omega_\mathbf{q}, q)F_{ss}^{(j)}(\omega_\mathbf{q}, q)\mathcal{N}_B(\omega_\mathbf{q}), \tag{10}$$

where $\tilde{V}(q) = V_0(q)/\epsilon(\omega_\mathbf{q}, q)$, $\mathcal{N}_B(\omega) = n_B(\omega - \Delta\mu_{eh}) - n_B(\omega)$, and the frequency of virtual photon is at the edge of the excitation cone, $\omega_\mathbf{q} = v_0 q$. The factorization allows one to evaluate and discuss the effect of a particular band structure and that of statistics independently.

We first discuss the geometry of intragroup AR enabled by in-plane velocity anisotropy, assuming the principal axis of the Weyl velocity tensor is parallel to the crystallographic ones. In the W_1 node group of TaAs, there exist four Weyl velocity tensors with pairwise perpendicular dispersion surfaces. For each such pair, the geometric part $\mathcal{G}_{xy}$ is given by volume between two ellipsoids in $\mathbf{q}$ space, as illustrated in Fig. 2(c). Explicit calculation in the limit $|v_x - v_y| \ll v_\perp = (v_x + v_y)/2$ results in [38]

$$\mathcal{G}_{xy} = \frac{|v_x - v_y|}{v_\perp} g\big(1 - v_z^2/v_\perp^2\big)\left(\frac{v_z}{v_\perp}\right)^{5/3}, \tag{11}$$

$$g(x) = \frac{\sqrt{x(1-x)} + (2x-1)\arctan\sqrt{\frac{x}{1-x}}}{(1-x)x^{3/2}}. \tag{12}$$

The AR rate also does not vanish even if node dispersions differ in tilt only. The tilt-enabled geometric factor $\mathcal{G}_t$ is given by the volume between two shifted spheres in $\mathbf{q}$ space, as shown in Fig. 2(e), so that

$$\mathcal{G}_t = \frac{\pi|\mathbf{u}^{(i)} - \mathbf{u}^{(j)}|}{v_0}, \tag{13}$$

where $\mathbf{u}^{(i,j)} = \mathbf{u}_{n,n'}g_{n,n'}^{(i,j)}$, $i, j \in W_{n,n'}$, and we have assumed equal velocity tensors for different nodes.

When there exist multiple Weyl node groups, the difference in (averaged) Weyl velocities becomes a more important factor enabling AR than anisotropy and tilt. Neglecting the latter, the geometry term $\mathcal{G}_\circledcirc$ is given by volume between two spheres in q space, as shown in Fig. 2(d), and results in

$$\mathcal{G}_\circledcirc = \frac{8\pi(v_2 - v_1)\theta(v_2 - v_1)}{v_1 + v_2}. \tag{14}$$

A striking feature of internode AR is its *nonreciprocity*, i.e., the absence of recombination in the group with fastest Weyl velocity $v_\star$. Indeed, the virtual photon with momentum $q < \omega/v_\star$ emitted upon e-h annihilation in the "fast" group cannot be absorbed in "slow" nodes (while the opposite is possible). Thus, this peculiar fast node is *geometrically protected* from

TABLE I. Summary of results for relaxation dynamics of excited carrier density $p(t)$ in WSM with single node group. μ is the equilibrium Fermi energy and $C(\alpha_\eta)$ are dimensionless screening functions depending on coupling constant $\alpha_\eta = \eta e^2/\varkappa v_0$ listed in [38].

	Strong pumping $\Delta\mu_{eh} \gg T$	Weak pumping $\Delta\mu_{eh} \ll T$
	Subexponential	
Intrinsic	$p/p_0 = (1 + t/3\tau_0)^{-3}$	Exponential
$\mu = 0$	$\tau_0 = \dfrac{\eta^{4/3}}{C_{1d}(\alpha_\eta)\mathcal{G}_1 v_0 p_0^{1/3}}$	$\tau = \dfrac{\eta}{C_{1n}(\alpha_\eta)\mathcal{G}_1 T}$
	Superexponential	
Extrinsic	$p/p_0 = (1 - t/3\tau_0)^3$	Exponential
$\mu \gg T$	$\tau_0 = \dfrac{v_0\eta^{2/3}p_0^{1/3}}{C_{2d}(\alpha_\eta)\mathcal{G}_1\mu^2}$	$\tau = \dfrac{\eta T}{C_{2n}(\alpha_\eta)\mathcal{G}_1\mu^2}$

AR, provided the anisotropy and tilt are weak. Below we show that geometrical protection elongates the nonradiative lifetime in real WSMs up to several nanoseconds.

IV. TEMPORAL DYNAMICS OF POPULATION INVERSION

Once the interband population inversion is created in WSMs, its relaxation after relatively fast intraband equilibration (due to electron-electron scattering) is governed by the interband processes. Assuming that the AR lifetime in WSMs is shorter than the phonon-limited lifetime [40], we consider the temporal dynamics with AR channel only,

$$\frac{dp_n}{dt} = -\mathcal{R}_n, \tag{15}$$

where $\mathcal{R}_n = \sum_{\substack{i\in n \\ j,s}} \mathcal{R}_{ij}^{(s)}$ is a partial AR rate in W_n and $p_n(t) = n_n(t)$ are the nonequilibrium carrier densities at each node group W_n. Assuming uniform pumping at each node, we solve Eq. (15) with a given initial total nonequilibrium density p_0 distributed among the node groups according to their degeneracy factors η_n. For estimates, we take the average Weyl velocity $v_0 = 2.5 \times 10^7$ cm/s, $\varkappa = 10$, $T = 77$ K, and the geometry factors $\mathcal{G}_{1,2}$ for the intragroup and intergroup contributions as 0.1 and 0.2, respectively. The dielectric function $\epsilon(\omega, \mathbf{q})$ is adopted in Thomas-Fermi approximation [38].

The specific band structure of WSMs imprints on AR rates already in materials with a single node group (as expected in strained HgTe [41]). Particularly, the rate at strong pumping (quasi-Fermi level $\delta\mu \gg T$) never follows the p^3 law inherent to common semiconductors. The superseding dynamics is summarized in Table I and Fig. 3.

Strong deviations from p^3 law occur due to carrier degeneracy and screening. The latter is proportional to the total number of nodes $\eta = \sum_n \eta_n$ (24 in the TaAs family and 8 in strained HgTe). This makes the total AR rate (almost) independent of the nodal degeneracy and the lifetimes—nearly proportional to η, thus enhancing them by more than an order of magnitude. Strong pumping of intrinsic nodes (equilibrium Fermi level $\mu = 0$) results in subexponential relaxation, while strong pumping of extrinsic ones ($\mu \gg T$) results in superexponential relaxation. Recombination at weak

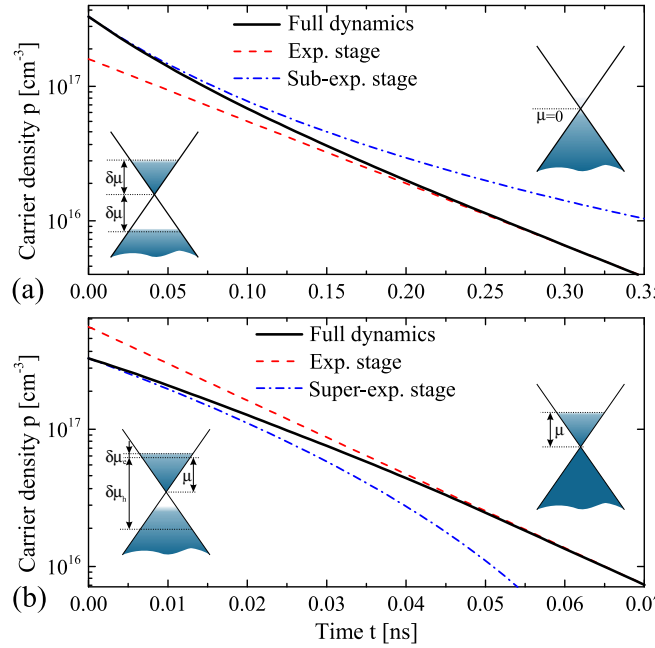

FIG. 3. Dynamics of the nonequilibrium carrier density $p(t)$ in WSMs with a sole node group ($p_0 = 3 \times 10^{17}$ cm^{-3}), intrinsic (a) and extrinsic (b) with residual density $n_r = 10^{18}$ cm^{-3} ($\mu \approx 25$ meV). The exponential (nondegenerate) and nonexponential (degenerate) analytical limits are shown by dashed lines. Insets show the band fillings right after intraband thermalization (left) and long after characteristic recombination time (right).

pumping and/or at final stages is, as expected, exponential. It is faster in extrinsic nodes by almost an order of magnitude due to the *parabolic* density of states in WSMs.

In multigroup WSMs the picture of relaxation becomes much more complicated [38]. The most remarkable feature of it is the *geometric protection* of population inversion in "fast" nodes. If all eigenvalues of the Weyl velocity tensor in W_1 exceed those in W_2, the intergroup channel of AR for W_1 is locked. Additionally, the intragroup channel is suppressed due to screening by the resident carriers at W_2. The band structure of TaAs, the first experimentally discovered WSM, favors such scenario. It possesses almost intrinsic 8-fold degenerate node group W_1, and extrinsic 16-fold degenerate node group W_2 with $\mu \approx 20$ meV [1]. Therefore, one can expect extralong lifetimes of carriers in W_1, which is further proved by our calculations in Fig. 4(a).

At the excitation density $p_0 = 3 \times 10^{17}$ cm^{-3} the distributions at both W_1 and W_2 are degenerate, and the evolution of $p_2(t)$ is given by equations of a superexponential case with η substituted by degeneracy of heavily occupied node η_2, while

$$p_1(t) = \frac{p_1(0)}{(1 + 5t/3\tau_0)^{3/5}}, \tag{16}$$

$$\tau_0^{-1} = C_{3n} v_0^5 \eta_2^{-2} \eta_1^{-2/3} \mathcal{G}_1 \mu^{-4} p_1(0)^{5/3} \tag{17}$$

with $C_{3n} \approx 234$. In the nondegenerate limit of carrier distribution in W_1 and the valence band of W_2, the relaxation is exponential in both groups. The lifetime of carriers in W_2 is the same as in a doped single-group case with $\eta \to \eta_2$, while

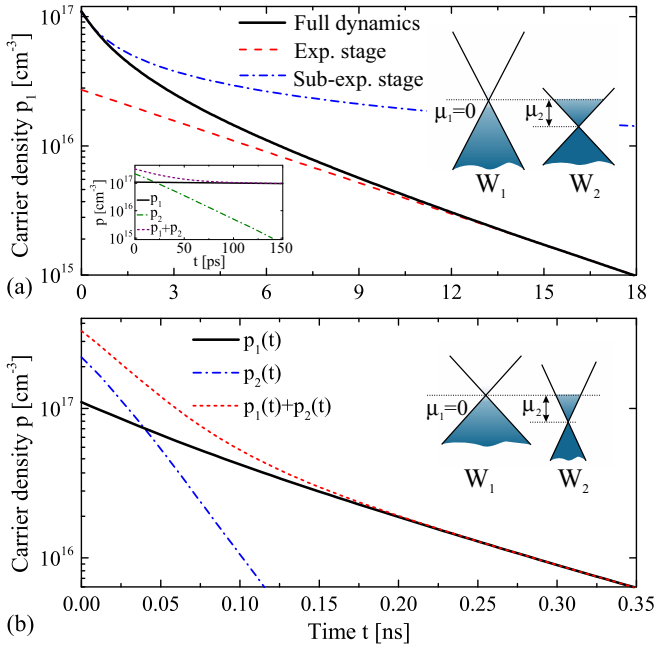

FIG. 4. Dynamics of the population inversion in WSMs with 8-fold degenerate intrinsic node group W_1 and 16-fold degenerate extrinsic group W_2 with (a) and without (b) *geometrical protection* of W_1 (either $v_1 > v_2$ or $v_1 < v_2$). The inset in (a) shows fast relaxation of p_2 in contrast to long-living $p_1(t)$. Diagrams on the right show the band occupancy at equilibrium.

for W_1

$$\tau^{-1} = C_{1n}(\beta_{\eta_2})\mathcal{G}_1\eta_1\eta_2{}^{-2}\alpha_{\eta_1}^2\beta_{\eta_2}^{-2}T, \tag{18}$$

where $\beta_{\eta_2} = (3/\pi^2)(\mu/T)^2\alpha_{\eta_2}$. Numerical evaluation of Eq. (15) for $p_{1,2}(t)$ [see Fig. 4(a)] illustrates that in both cases the lifetimes of *geometrically protected* carriers are by the orders of magnitude larger than those in single-group WSMs (Fig. 3), the lifetimes of carriers of W_2 [inset in Fig. 4(a)], or when the intrinsic node group is unprotected [38] [$v_1 < v_2$, Fig. 4(b)].

V. DISCUSSION AND CONCLUSIONS

We have shown that peculiar ultrarelativistic band structure of WSMs leads to strong suppression of AR due to phase space restrictions imposed by energy and momentum conservation. The only allowed Auger process involves scattering between Weyl nodes with dissimilar carrier dispersion laws. In comparison to graphene, the carrier lifetimes in realistic WSM are elongated by several orders of magnitude thanks to (1) "geometrical" restrictions in phase space and (2) strong screening of Coulomb interaction proportional to the number of nodes.

The most striking feature of the intergroup AR in WSMs is the *geometrical protection* of the population inversion in the "fastest" node group $W_\star$, where the rate of this process vanishes. The persistent recombination channels due to velocity anisotropy and tilt can be strongly suppressed if $W_\star$ is intrinsic and there are enough carriers outside of it to provide strong screening. As a result, the lifetimes up to 10^{-8} s can be achieved in WSM with *geometrically protected* node group. Experimental studies of TaAs support the desired band structure, so the proposed scenario is highly realistic. These lifetimes are five orders of magnitude longer than those reported experimentally for two-dimensional graphene ($\tau_r \sim 130$ fs [42]) and theoretically for three-dimensional gapless HgTe ($\tau_r \sim 100 \ldots 500$ fs [43]). They also exceed the recombination lifetimes in several gapped materials: CdHgTe quantum wells ($E_g = 14$ meV, $\tau_r \sim 60$ ps [44]) and bulk PbSe ($E_g = 170$ meV, $\tau_r \sim 0.5 \ldots 2$ ns [45]).

In real WSM, bulk Weyl nodes coexist with parabolic bands occupied by nondegenerate holes with density p^*. This opens up a recombination channel with virtual photon absorption in parabolic band. It is possible to show that such process demonstrates activation-type behavior $\mathcal{R} \propto p^* e^{-E_{th}/T}$ with $E_{th} = m^* v_0^2/2$ and m^* being the effective mass. Taking $m^* = 0.4m_0$, we obtain $E_{th} \approx 70$ meV, which justifies the irrelevance of such recombination process at room temperature.

In all WSMs, there exist surface states with arclike dispersion connecting the projections of bulk Weyl points onto the surface Brillouin zone (Fermi arcs) [5–8]. Recombination involving surface states is not suppressed by energy-momentum conservation, but suppressed due to localization of the arc states' wave function near the surface [46]. The ratio of bulk and surface recombination rates can be roughly estimated as $k_F L$, where L is the sample size and k_F is the Fermi wave vector.

Our preliminary estimates show that account of dynamic screening further suppresses AR, as the real part of the screening function has a logarithmic singularity at the edge of the excitation cone [47]. This would result in an extra large log factor in carrier lifetime, of the order of $\ln^2 \mathcal{G}^{-1}$. All these results allow us to consider WSMs as promising candidates for long-lasting nonequilibrium states and efficient coherent terahertz emission.

ACKNOWLEDGMENTS

This work was supported by Grants No. 16-37-60110 and No. 16-29-03402 of the Russian Foundation for Basic Research. D.S. acknowledges the support from Research Institute for Electrical Communication, Tohoku University (Grant No. H29/A11 for Nation-Wide Cooperative Research Projects).

[1] N. P. Armitage, E. J. Mele, and A. Vishwanath, Rev. Mod. Phys. **90**, 015001 (2018).
[2] G. E. Volovik, *The Universe in a Helium Droplet* (Oxford University Press, New York, 2003), Vol. 117.
[3] S. R. Elliott and M. Franz, Rev. Mod. Phys. **87**, 137 (2015).
[4] K. S. Novoselov, A. K. Geim, S. Morozov, D. Jiang, M. Katsnelson, I. Grigorieva, S. Dubonos, and A. Firsov, Nature (London) **438**, 197 (2005).

[5] B. Q. Lv, H. M. Weng, B. B. Fu, X. P. Wang, H. Miao, J. Ma, P. Richard, X. C. Huang, L. X. Zhao, G. F. Chen, Z. Fang, X. Dai, T. Qian, and H. Ding, Phys. Rev. X **5**, 031013 (2015).

[6] S.-Y. Xu, I. Belopolski, N. Alidoust, M. Neupane, G. Bian, C. Zhang, R. Sankar, G. Chang, Z. Yuan, C.-C. Lee, S.-M. Huang, H. Zheng, J. Ma, D. S. Sanchez, B. Wang, A. Bansil, F. Chou, P. P. Shibayev, H. Lin, S. Jia, and M. Z. Hasan, Science **349**, 613 (2015).

[7] S.-Y. Xu, I. Belopolski, D. S. Sanchez, C. Zhang, G. Chang, C. Guo, G. Bian, Z. Yuan, H. Lu, T.-R. Chang, P. P. Shibayev, M. L. Prokopovych, N. Alidoust, H. Zheng, C.-C. Lee, S.-M. Huang, R. Sankar, F. Chou, C.-H. Hsu, H.-T. Jeng, A. Bansil, T. Neupert, V. N. Strocov, H. Lin, S. Jia, and M. Z. Hasan, Sci. Adv. **1**, 1501092 (2015).

[8] S.-Y. Xu, N. Alidoust, I. Belopolski, Z. Yuan, G. Bian, T.-R. Chang, H. Zheng, V. N. Strocov, D. S. Sanchez, G. Chang, C. Zhang, D. Mou, Y. Wu, L. Huang, C.-C. Lee, S.-M. Huang, B. Wang, A. Bansil, H.-T. Jeng, T. Neupert, A. Kaminski, H. Lin, S. Jia, and M. Zahid Hasan, Nat. Phys. **11**, 748 (2015).

[9] Z. K. Liu, B. Zhou, Y. Zhang, Z. J. Wang, H. M. Weng, D. Prabhakaran, S.-K. Mo, Z. X. Shen, Z. Fang, X. Dai, Z. Hussain, and Y. L. Chen, Science **343**, 864 (2014).

[10] M. Neupane, S.-Y. Xu, R. Sankar, N. Alidoust, G. Bian, C. Liu, I. Belopolski, T.-R. Chang, H.-T. Jeng, H. Lin *et al.*, Nat. Commun. **5**, 3786 (2014).

[11] N. Stander, B. Huard, and D. Goldhaber-Gordon, Phys. Rev. Lett. **102**, 026807 (2009).

[12] Y. Wang, D. Wong, A. V. Shytov, V. W. Brar, S. Choi, Q. Wu, H.-Z. Tsai, W. Regan, A. Zettl, R. K. Kawakami, S. G. Louie, L. S. Levitov, and M. F. Crommie, Science **340**, 734 (2013).

[13] C.-L. Zhang, S.-Y. Xu, I. Belopolski, Z. Yuan, Z. Lin, B. Tong, G. Bian, N. Alidoust, C.-C. Lee, S.-M. Huang *et al.*, Nat. Commun. **7**, 10735 (2016).

[14] J. Gooth, A. C. Niemann, T. Meng, A. G. Grushin, K. Landsteiner, B. Gotsmann, F. Menges, M. Schmidt, C. Shekhar, V. Suss, R. Huhne, B. Rellinghaus, C. Felser, B. Yan, and K. Nielsch, Nature (London) **547**, 324 (2017).

[15] T. Liang, Q. Gibson, M. N. Ali, M. Liu, R. Cava, and N. Ong, Nat. Mater. **14**, 280 (2015).

[16] A. S. Mayorov, R. V. Gorbachev, S. V. Morozov, L. Britnell, R. Jalil, L. A. Ponomarenko, P. Blake, K. S. Novoselov, K. Watanabe, T. Taniguchi, and A. K. Geim, Nano Lett. **11**, 2396 (2011).

[17] O. V. Kibis, Europhys. Lett. **107**, 57003 (2014).

[18] L. Keldysh, Contemp. Phys. **27**, 395 (1986).

[19] C. Triola, A. Pertsova, R. S. Markiewicz, and A. V. Balatsky, Phys. Rev. B **95**, 205410 (2017).

[20] N. H. Lindner, G. Refael, and V. Galitski, Nat. Phys. **7**, 490 (2011).

[21] J. Iveland, L. Martinelli, J. Peretti, J. S. Speck, and C. Weisbuch, Phys. Rev. Lett. **110**, 177406 (2013).

[22] S. V. Morozov, V. V. Rumyantsev, M. A. Fadeev, M. S. Zholudev, K. E. Kudryavtsev, A. V. Antonov, A. M. Kadykov, A. A. Dubinov, N. N. Mikhailov, S. A. Dvoretsky, and V. I. Gavrilenko, Appl. Phys. Lett. **111**, 192101 (2017).

[23] A. R. Adams, Electron. Lett. **22**, 249 (1986).

[24] G. E. Cragg and A. L. Efros, Nano Lett. **10**, 313 (2010).

[25] M. Nawrocki, Y. G. Rubo, J. P. Lascaray, and D. Coquillat, Phys. Rev. B **52**, R2241 (1995).

[26] F. Arnold, C. Shekhar, S.-C. Wu, Y. Sun, R. D. dos Reis, N. Kumar, M. Naumann, M. O. Ajeesh, M. Schmidt, A. G. Grushin, J. H. Bardarson, M. Baenitz, D. Sokolov, H. Borrmann, M. Nicklas, C. Felser, E. Hassinger, and B. Yan, Nat. Commun. **7**, 11615 (2016).

[27] J. Hu, J. Y. Liu, D. Graf, S. M. A. Radmanesh, D. J. Adams, A. Chuang, Y. Wang, I. Chiorescu, J. Wei, L. Spinu, and Z. Q. Mao, Sci. Rep. **6**, 18674 (2016).

[28] J. Klotz, S.-C. Wu, C. Shekhar, Y. Sun, M. Schmidt, M. Nicklas, M. Baenitz, M. Uhlarz, J. Wosnitza, C. Felser, and B. Yan, Phys. Rev. B **93**, 121105 (2016).

[29] P. R. Emtage, J. Appl. Phys. **47**, 2565 (1976).

[30] O. Ziep and M. Mocker, Phys. Status Solidi B **98**, 133 (1980).

[31] P. A. M. Dirac, Math. Proc. Cambridge Philos. Soc. **26**, 361 (1930).

[32] L. Fritz, J. Schmalian, M. Muller, and S. Sachdev, Phys. Rev. B **78**, 085416 (2008).

[33] F. Rana, Phys. Rev. B **76**, 155431 (2007).

[34] T. Winzer and E. Malic, Phys. Rev. B **85**, 241404 (2012).

[35] A. Tomadin, D. Brida, G. Cerullo, A. C. Ferrari, and M. Polini, Phys. Rev. B **88**, 035430 (2013).

[36] G. Alymov, V. Vyurkov, V. Ryzhii, A. Satou, and D. Svintsov, Phys. Rev. B **97**, 205411 (2018).

[37] We note that Eq. (1) incorporates both Auger recombination and generation processes, therefore it vanishes in equilibrium.

[38] See Supplemental Material at http://link.aps.org/supplemental/10.1103/PhysRevB.99.115202 for (I) evaluation of WSM polarizability, (II) factorization of AR rate, (III) evaluation of $\mathcal{G}$ for various shapes of dispersion surfaces, (IV) evaluation of $\mathcal{S}$ and screening functions in various pumping regimes, and (V) discussion of relaxation in multigroup WSMs.

[39] A. A. Abrikosov and S. D. Beneslavskii, Zh. Eksp. Teor. Fiz. **59**, 1280 (1970) [Sov. Phys. JETP **32**, 699 (1971)].

[40] S. Huang, M. Sanderson, J. Tian, Q. Chen, F. Wang, and C. Zhang, J. Phys. D: Appl. Phys. **51**, 015101 (2018).

[41] J. Ruan, S.-K. Jian, H. Yao, H. Zhang, S.-C. Zhang, and D. Xing, Nat. Commun. **7**, 11136 (2016).

[42] I. Gierz, M. Mitrano, J. C. Petersen, C. Cacho, I. C. E. Turcu, E. Springate, A. Stöhr, A. Köhler, U. Starke, and A. Cavalleri, J. Phys.: Condens. Matter **27**, 164204 (2015).

[43] M. I. D'yakonov and A. V. Khaetskii, Fiz. Tekh. Poluprovdn. **14**, 1499 (1980) [Sov. Phys. Semicond. **14**, 891 (1980)].

[44] S. V. Morozov, M. S. Joludev, A. V. Antonov, V. V. Rumyantsev, V. I. Gavrilenko, V. Y. Aleshkin, A. A. Dubinov, N. N. Mikhailov, S. A. Dvoretskiy, O. Drachenko, S. Winnerl, H. Schneider, and M. Helm, Semiconductors **46**, 1362 (2012).

[45] R. Klann, T. Höfer, R. Buhleier, T. Elsaesser, and J. W. Tomm, J. Appl. Phys. **77**, 277 (1995).

[46] Z. A. Devizorova and V. A. Volkov, Phys. Rev. B **95**, 081302 (2017).

[47] M. Lv and S.-C. Zhang, Int. J. Mod. Phys. B **27**, 1350177 (2013).